Magnetic Resonance Imaging 57 (2019) 277–284

Contents lists available at ScienceDirect

Magnetic Resonance Imaging

journal homepage: www.elsevier.com/locate/mri

Technical note

Novel distortion correction method for diffusion-weighted imaging based on non-rigid image registration between low b value image and anatomical image

Yasuo Takatsu[a,b,*], Hajime Sagawa[c], Masafumi Nakamura[d], Yuichi Suzuki[e], Tosiaki Miyati[b]

[a] Department of Radiological Technology, Faculty of Health and Welfare, Tokushima Bunri University, 1314-1 Shido, Sanuki-City, Kagawa 769-2193, Japan
[b] Division of Health Sciences, Graduate School of Medical Sciences, Kanazawa University, 5-11-80 Kodatsuno, Kanazawa, 920-0942, Japan
[c] Division of Clinical Radiology Service, Kyoto University Hospital, 54 Kawaharacho, Shogoin, Sakyo-ku, Kyoto 606-8507, Japan
[d] Department of Radiology, Otsu City Hospital, 2-9-9, Motomiya, Otsu-City, Shiga 520-0804, Japan
[e] Department of Radiology, The University of Tokyo Hospital, 7-3-1 Hongo, Bunkyo-ku, Tokyo 113-8655, Japan

ARTICLE INFO

Keywords:
Magnetic resonance imaging
Diffusion-weighted imaging
Distortion
Non-rigid image registration
Breast

ABSTRACT

Purpose: This study aimed to develop a novel technique for retrospective distortion correction based on non-rigid image registration in magnetic resonance diffusion image.

Methods: A 3.0 T MRI scanner with an 18-channel dedicated breast coil and the outer shell of the original breast phantom, which provided images with non-uniform fat-suppression based on clinical data were used. The diffusion-weighted imaging with and without parallel imaging (PI) was used.

The proposed study included several steps, which are FOV size matching, matrix size matching, image segmentation, edge detection, non-rigid image registration, and image wrap. We compared the results obtained using the proposed method with that obtained using TOPUP images. The correlation was assessed between T1-weighted image with fat suppression (FS-T1WI) and b1000 image with the help of cross-correlation coefficient (CCC). Shape-error analysis of tumor model and apparent diffusion coefficient (ADC) was calculated. The Steel–Dwass multiple-comparison tests were used for all comparisons and statistical analysis ($P < 0.05$).

Results: The novel method of CCC showed the highest correlation between FS-T1WI and b1000 images. In the Steel–Dwass multiple-comparison test, significant differences were found ($P < 0.05$) except between non-correction and TOPUP ($P = 0.99$).

The novel method was the lowest degree of error. With PI in the right breast, no significant differences, whereas in the left breast, significant differences were observed except for between novel method and TOPUP ($P = 0.73$). Without PI in the right breast, significant differences were observed. In the left breast, no significant differences were observed between any combinations.

The ADC value, no significant differences were observed for non-correction and novel methods.

Conclusions: We developed a novel technique for retrospective distortion correction based on non-rigid image registration. The high degree of accuracy of this method combined with the lack of requirement for additional scans renders it a promising tool for application in clinical practice.

1. Introduction

Diffusion-weighted imaging (DWI) and apparent diffusion coefficient (ADC) maps are widely used for the evaluation of acute brain infarction and the assessment of tumor differentiation and/or treatment effect. They play a vital role in magnetic resonance imaging (MRI).

For DWI, a motion-probing gradient (MPG) is used as a bipolar gradient for application in at least three directions. Echo planar imaging (EPI) is used owing to its faster scanning time. However, when EPI is used, image distortion may appear due to magnetic field inhomogeneity and eddy currents. One of the reasons for susceptibility is air. Therefore, surrounding air of the breast, intestinal gas, and paranasal sinus are influenced while performing breast, body, and face MRI, respectively. Distortion may be partially reduced using parallel imaging

* Corresponding author at: Department of Radiological Technology, Faculty of Health and Welfare, Tokushima Bunri University, 1314-1 Shido, Sanuki-City, Kagawa 769-2193, Japan.
E-mail addresses: ytakatsu@kgw.bunri-u.ac.jp (Y. Takatsu), hsagawa1109@gmail.com (H. Sagawa), nakamura-xx@leto.eonet.ne.jp (M. Nakamura), yuiti4038@yahoo.co.jp (Y. Suzuki), ramiyati@mhs.mp.kanazawa-u.ac.jp (T. Miyati).

https://doi.org/10.1016/j.mri.2018.12.002
Received 8 November 2018; Received in revised form 2 December 2018; Accepted 8 December 2018

(PI) [1]. Therefore, tumor position and/or shape may differ between DWI and anatomical image, such as T1-weighted image (T1WI) and T2-weighted image (T2WI).

In breast MRI, when the dynamic image was analyzed by the time intensity curve, setting the region of the interest (ROI) was essential. Therefore, in this study, we surmised that high-signal area in the b1000 image was compared with the enhanced area in the T1WI with fat suppression (FS-T1WI) obtained with contrast medium during breast MRI. Moreover, when ADC of the tumor was calculated, misalignment seemed to be severe problem from the viewpoint of setting the ROI. Hence, distortion correction should be performed in practice.

When EPI is used, the popular techniques for distortion correction include the use of a field map [2] and distortion correction in double images, which is performed by swapping the polarity of the phase-encoding direction (TOPUP) [3]. These techniques require a field map or polarity images to be obtained during scanning. Performing an extra scan may extend the total examination time, thereby resulting in fatigue in patients.

The use of non-rigid image registration for distortion correction, which is similar to the other technique, was reported [4,5]. This technique was applied for functional MRI (fMRI) [4]. Herein, we developed a novel technique for retrospective distortion correction based on the use of non-rigid image registration without the need for additional breast scans.

2. Materials and methods

2.1. Ethical consideration

Because this was a phantom study, Institutional Review Board's approval was not required.

2.2. MRI

A 3.0-T MRI scanner with an 18-channel dedicated breast coil (Prisma fit, VE11; Siemens Healthcare GmbH, Erlangen, Germany) was used. The sequence used was as follows: field of view (FOV), 330 mm; slice thickness, 3 mm; number of slices, 48; and fat-suppression technique, spectrally adiabatic inversion recovery. Parallel acquisition technique (PAT) of a generalized auto-calibrating partially parallel acquisition (GRAPPA) was performed to achieve PI. Moreover, FS-T1WI, as an anatomical image, was included in routine breast MRI protocol. These images were less distorted in comparison with EPI.

In general, ADC is calculated using images with low and high b values. We used no MPG (b0) and b1000 DWI; repetition time (TR), 7100 ms; echo time (TE), 45 ms; flip angle (FA), 90 °; matrix, 160 × 160; PAT factor, 2; band width (BW), 2404 Hz/pixel; phase encode direction (PED), posterior-to-anterior (PA); b value, 0 and 1000. FS-T1WI; volumetric interpolated breath-hold examination (VIBE); TR, 3.98 ms; TE, 1.5 ms; matrix, 384 × 384; PAT factor, 3; BW, 500 Hz/pixel; PED, RL. Non-PI DWI; TR, 8800 ms; TE, 75 ms; FA, 90 degrees; matrix, 160 × 160; PAT factor, off; BW, 2404 Hz/pixel; PED, PA; b value, 0 and 1000. Each scan was performed for five times continuously.

In general, PI is used with DWI to reduce distortion. In this study, DWI was performed with and without PI to assess whether the novel method was effective in correcting severe image distortion without the use of PI.

2.3. Phantom

The outer shell of the original breast phantom, which provided images with non-uniform fat-suppression based on clinical data, was formed using a thermoplastic sheet for radiotherapy (457 × 559 mm, thickness: 3.2 mm, HipFix Thermoplastic, MTHFX1822S; MEDTEC, Inc., DBA CIVCO Medical Solutions and CIVCO Radiotherapy, Coralville, IA, USA). This outer shell was the same as the one used in previous studies [6,7] (Fig. 1).

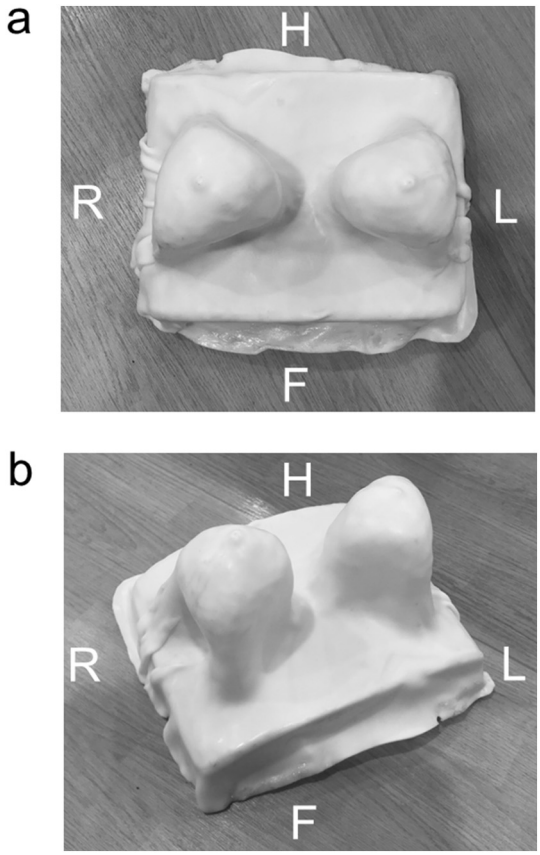

Fig. 1. Images of the phantom.
Outer shell of the phantom made of a radiotherapy shell (a, b).
H, head direction; F, foot direction; R, right direction; L, left direction.

The phantom included salad oil (as fat), 1500 mL; water, 1500 mL; liquid detergent, 300 mL; and a thickener consisting of 66.67% maltodextrin and 33.33% xanthan gum (rich-powder; Fantasy, Inc., Saitama, Japan), 10 g. The T1 and T2 relaxation times were 697.0 and 102.1 ms, respectively.

The mammary tumor model (gadoteridol [Prohance, Eisai, Tokyo, Japan], 0.5 mM; dextrin, 30%w/v; T1 relaxation time, 286.0 ms; T2 relaxation time, 54.7 ms; ADC, 1.087 × 10^3 mm^2/s) was in the form of an acryl sphere (65 mmφ).

2.4. Correction technique

A novel method based on a non-rigid image registration was performed using the b0 image, which was transformed to match up with the anatomical image. Moreover, the displacement field between both images was created. Distortion correction was performed by applying the displacement field to an image with high b value. The numerical analysis software used was, Matlab (version 2018a, MathWorks, Inc., Massachusetts, USA).

The study proceeded through the following steps:

(1) FOV size matching

The FOV size was assumed to differ between DWI (both b0 and b1000 images) and the anatomical image. The zero-fill interpolation was performed to match FOV size to these images.

(2) Matrix size matching

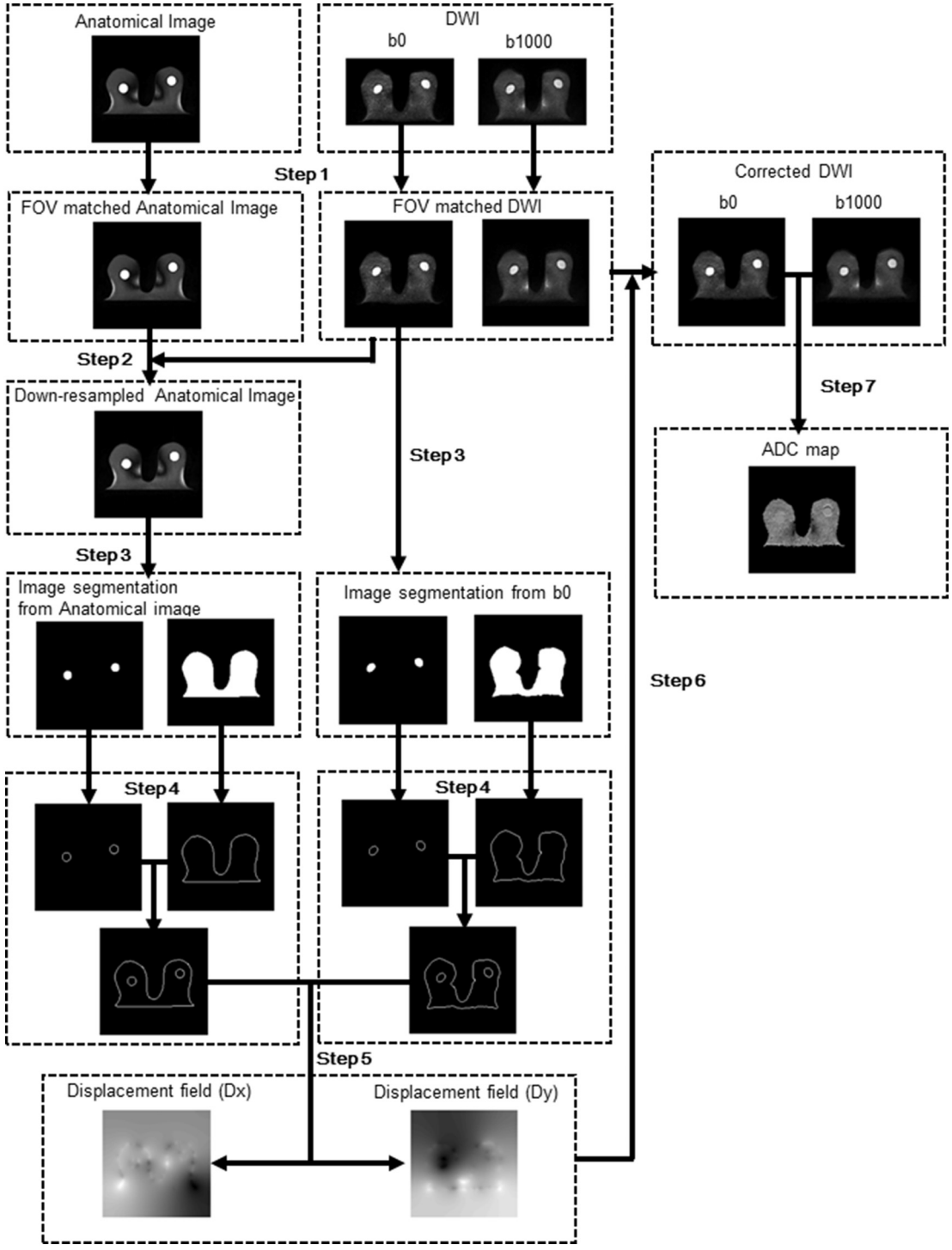

Fig. 2. Procedure of the correction technique.

In general, the matrix size of DWI (both b0 and b1000 images) was lower than that of the anatomical image. Therefore, the down-resampling of the anatomical image was performed to match the matrix size between DWI and anatomical image. The anatomical image was transformed to frequency space by Fourier transform. The surrounding area was removed, and the central area was obtained by down-resampling. After that, inverse Fourier transform was performed.

(3) Image segmentation

Gaussian-filtered images from b0 and anatomical images were created to avoid the influence of the noise. The plural threshold value was set at these images, and the image was segmented. If the quality of segmentation could be increased, plural anatomical images with varying degrees of contrast were obtained.

(4) Edge detection

The edge was detected in the image from step (3) using Sobel filter. The edge addition process was performed to both low b value and anatomical images. This process was conducted using the fast computation time and by avoiding excessive deformation in the next step.

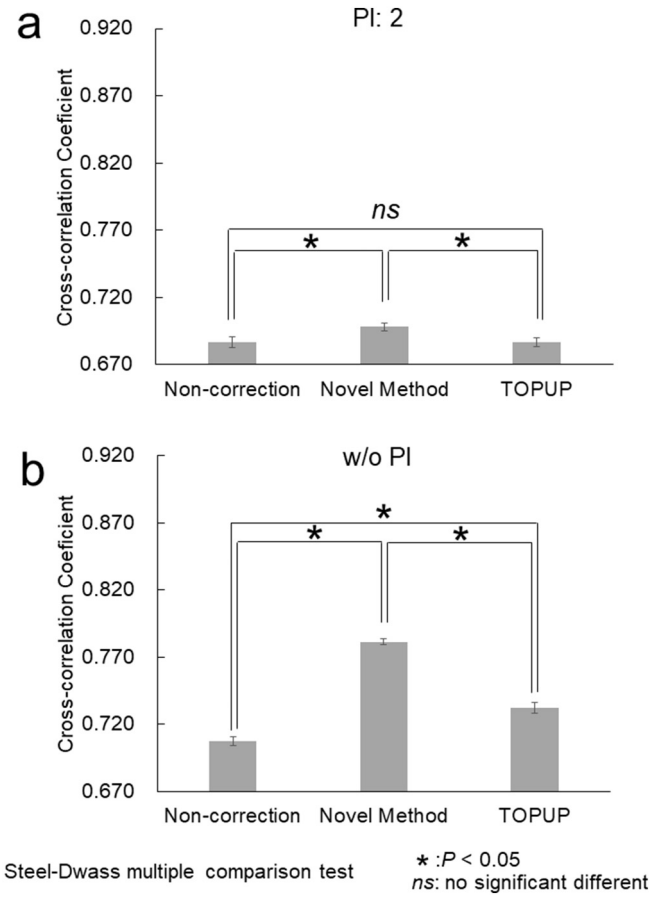

Fig. 3. Cross-correlation coefficient (CCC).
CCC was assessed between T1-weighted image with fat suppression and b1000 images with (a) and without (b) parallel imaging (PI). PI factor was 2.

(5) Non-rigid image registration

Using the edge image acquired in step (4), non-rigid image registration was performed using an edge image with a low b value and an edge image of the anatomical image using the Demons algorism [8,9]. Thus, displacement field (x direction, Dx; y direction, Dy) was obtained. During this procedure, the number of pyramid was three, and the number of iteration times was 500.

(6) Image warp

Obtained displacement field, as obtained in step (5), was applied to b1000 image to warp and correct distortion, as shown in Fig. 2.

2.5. ADC map calculation

The ADC map was created by distortion corrected b0 and b1000 images.

The ADC map was calculated using the following equation:

$$ADC = \frac{-In[S(b1000)/S(b0)]}{b1000 - b0},$$

where “S” is the signal intensity and “b0” and “b1000” are the b values.

2.6. TOPUP image

To confirm the validity of our results, we compared the results obtained using the novel method with that obtained using TOPUP images. The polarity of phase-encoding direction was swapped and TOPUP image was created. Using blip-up blip-down methods, FSL package [10] was used.

2.7. Assessment of correlation

The correlation between FS-T1WI and b1000 images was assessed using cross-correlation coefficient (CCC), which was calculated as follows:

$$CCC = \frac{\sum_m \sum_n (A_{mn} - \overline{A})(B_{mn} - \overline{B})}{\sqrt{(\sum_m \sum_n (A_{mn} - \overline{A})^2)(\sum_m \sum_n (B_{mn} - \overline{B})^2)}},$$

where “A” is the anatomical image (FS-T1WI) used for reference, “B” is the DWI (b1000 image), and “m” and “n” are the x and y coordinate of FOV, respectively.

CCC was performed to compare the non-correction image and corrected image using novel and TOPUP methods both with and without PI.

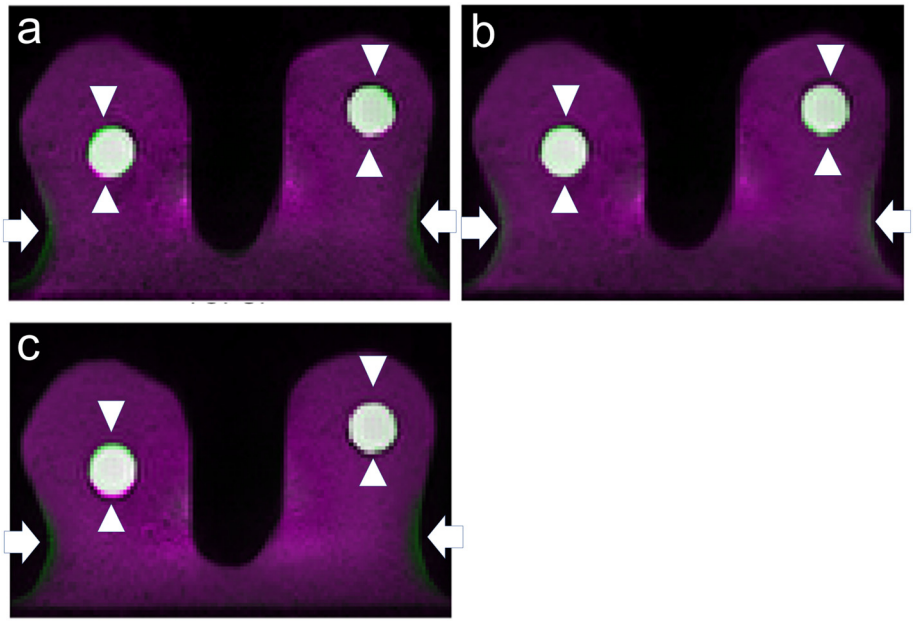

Fig. 4. Fusion images with parallel imaging (PI).
The fusion images of non-correction (a), novel method (b) and TOPUP (c) between T1-weighted image with fat suppression (green) and b1000 images (purple) were created with PI. The novel method correlated well with these data and fusion images (arrow and arrow head). (For interpretation of the references to color in this figure legend, the reader is referred to the web version of this article.)

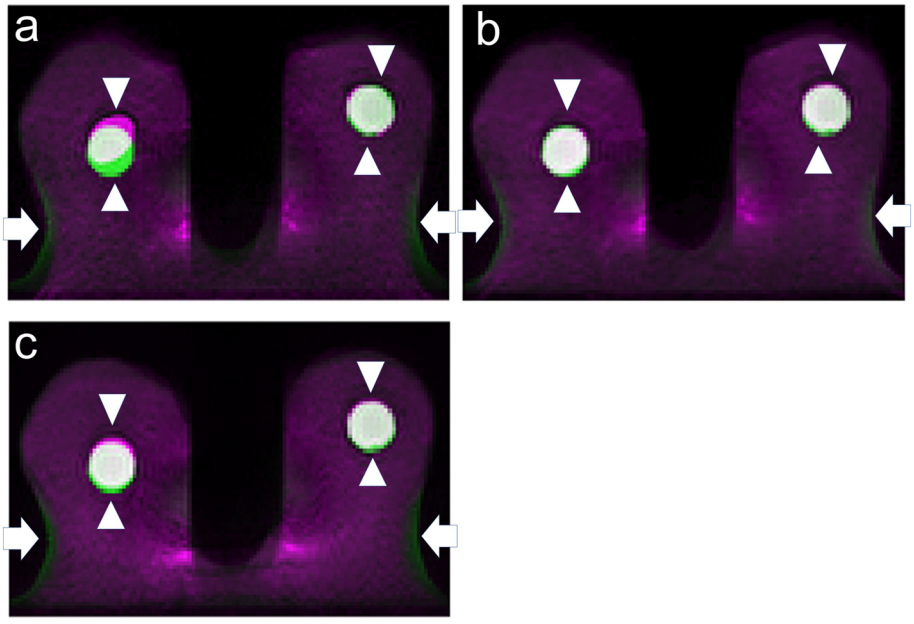

Fig. 5. Fusion images without parallel imaging (PI). The fusion images of non-correction (a), novel method (b) and TOPUP (c) between T1-weighted image with fat suppression (green) and b1000 images (purple) were created without PI. The novel method correlated well with these data and fusion images (arrow and arrow head). (For interpretation of the references to color in this figure legend, the reader is referred to the web version of this article.)

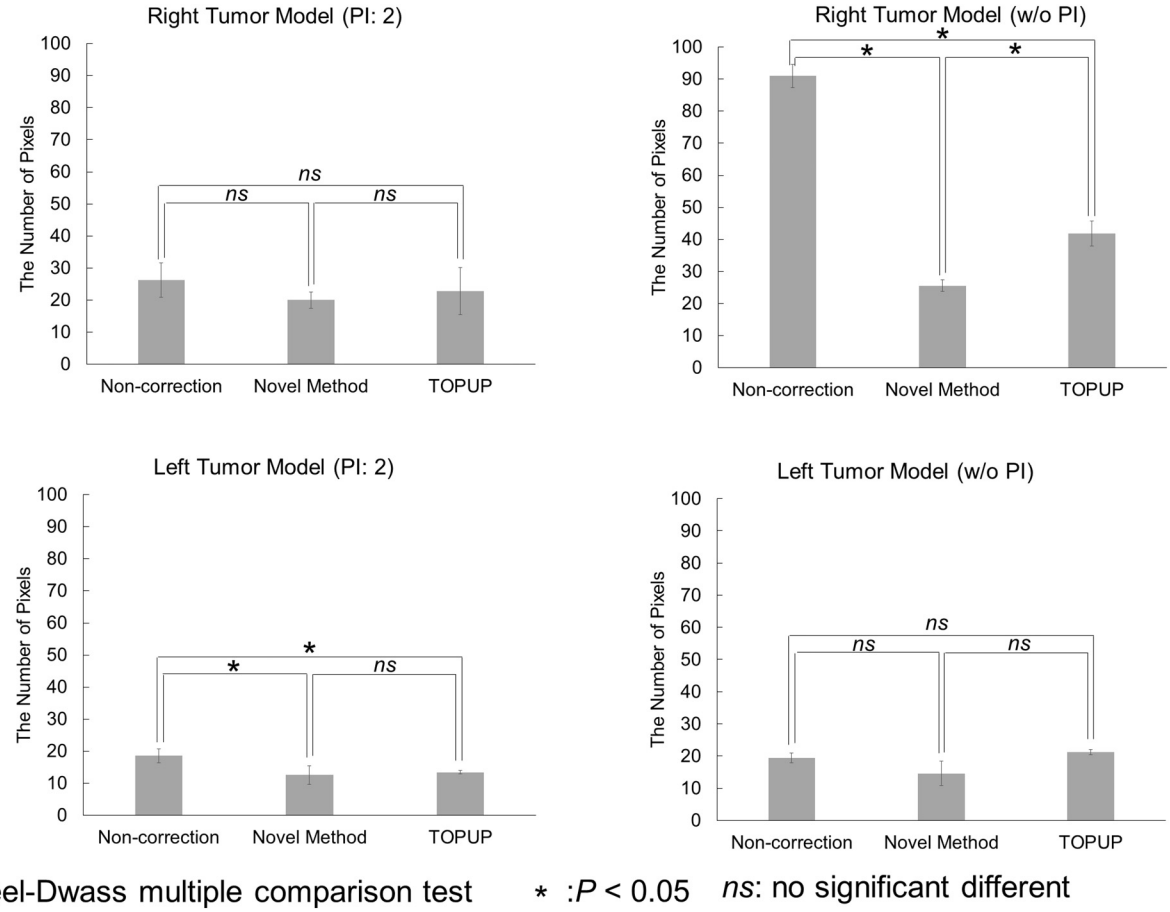

Fig. 6. Shape-error analysis.
Shape error of the tumor model was analyzed by binarizing T1-weighted image with fat suppression and b1000 images with and without parallel imaging (PI). PI factor was 2.

When the value of CCC was higher, the degree of correlation was higher.

Moreover, the fusion images between FS-T1WI and b1000 images were created.

2.8. Shape error analysis

Shape error of the tumor model was analyzed by binarizing FS-T1WI and b1000 images using P-tile thresholding. Thresholds were manually

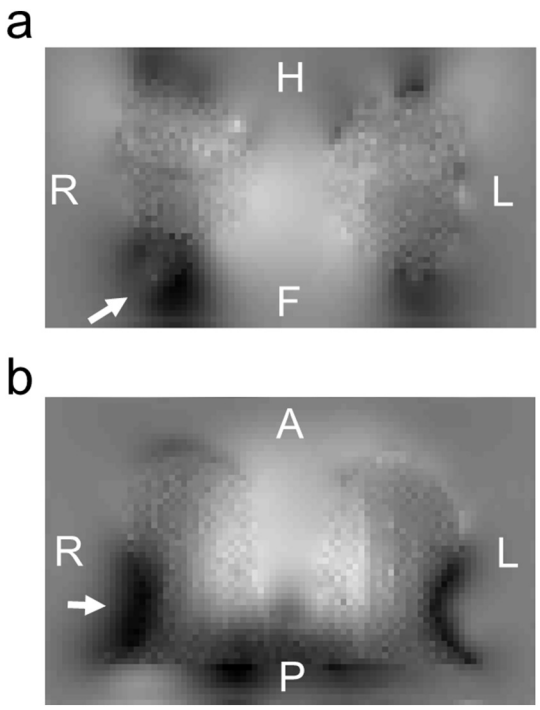

Fig. 7. Displacement field by TOPUP.
The right breast was inhomogeneous (arrow) (a, b).
H, head direction; F, foot direction; R, right direction; L, left direction.

adjusted to match the true size and were set to 83% in each image. Moreover, the difference between FS-T1WI and b1000 image was calculated. The non-correction, novel method, and TOPUP images were compared. When the value was smaller, error was smaller.

2.9. Comparison of ADC

ADC was compared between before and after correction. The size of the region of interest was > 50 pixels using freehand by Matlab. Non-correction, use of the novel method, and use of TOPUP images were compared.

2.10. Statistical analysis

The Kruskal–Wallis and Steel–Dwass multiple-comparison tests were used for all comparisons and statistical analysis ($P < 0.05$) (EZR v. 1.37 [11]).

3. Results

3.1. Assessment of correlation

This novel method of CCC showed the highest correlation between FS-T1WI and b1000 images with and without PI. In Kruskal–Wallis test, a significant difference was found with ($P < 0.01$) and without PI ($P < 0.01$). In the Steel–Dwass multiple-comparison test, significant differences were found ($P < 0.05$) except between non-correction and TOPUP ($P = 0.99$) with PI (Fig. 3). The proposed method correlated well with these data and fusion images (Figs. 4, 5).

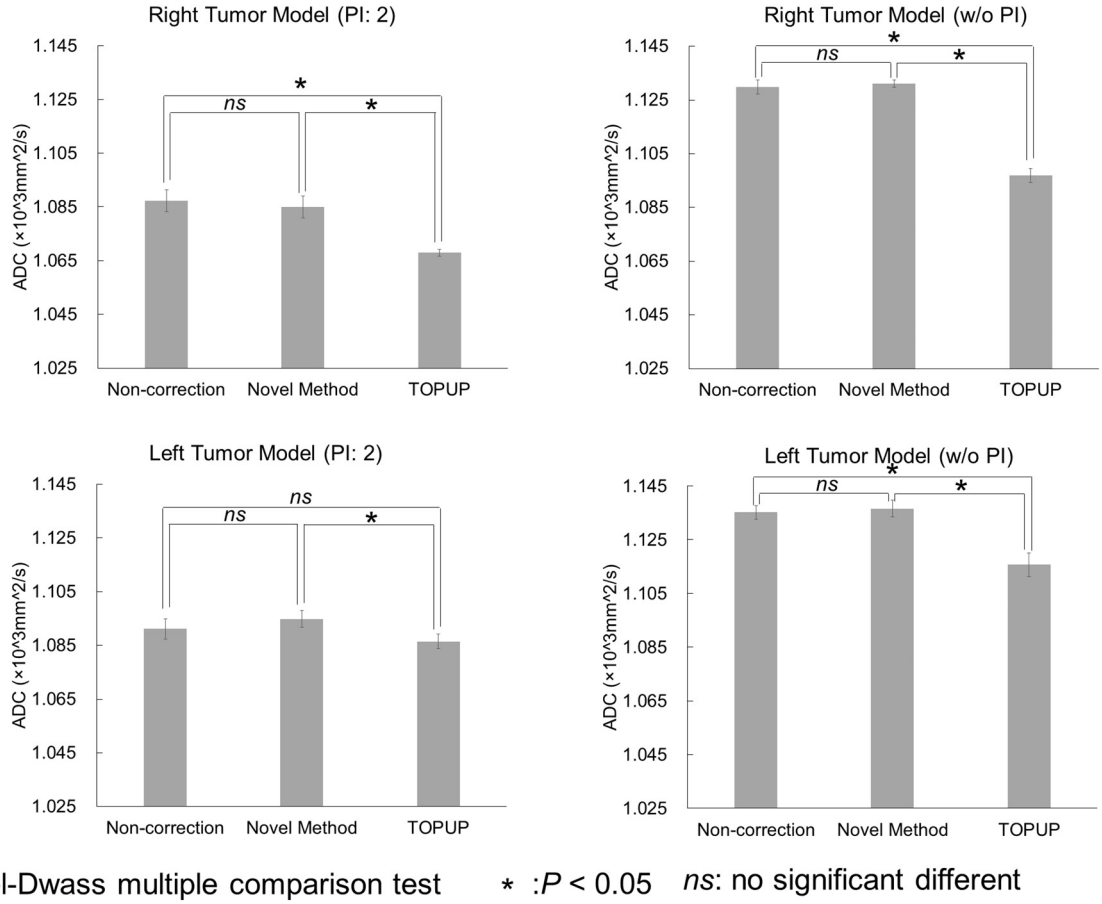

Fig. 8. Comparison of apparent diffusion coefficient (ADC).
ADC was compared between before (non-correction) and after correction with and without parallel imaging (PI). PI factor was 2.

3.2. Shape error analysis

For all the combinations that were investigated, the novel method presented here yielded the lowest degree of error. With PI in the right breast, no significant differences were observed in the Kruskal–Wallis test ($P = 0.21$), whereas in the left breast, significant differences were observed in the Kruskal–Wallis ($P < 0.05$) and Steel–Dwass multiple-comparison tests ($P < 0.05$) except for the differences observed between novel method and TOPUP ($P = 0.73$).

Without PI in the right breast, significant differences were observed in the Kruskal–Wallis ($P < 0.01$) and Steel–Dwass multiple-comparison tests ($P < 0.05$). In the left breast, significant differences were observed in the Kruskal–Wallis test ($P < 0.05$), although no significant differences were observed between any combinations in the Steel–Dwass multiple-comparison test. Without using PI for the right breast, the number of pixels increased (Fig. 6). The displacement field estimated from TOPUP of the right breast was inhomogeneous. (Fig. 7).

3.3. Comparison of ADC

The ADC value was lowest for TOPUP method. The Kruskal–Wallis test revealed significant differences from the results achieved with PI in the right breast ($P < 0.01$), whereas the Steel–Dwass multiple-comparison test did not reveal significant differences between non-correction and the novel method ($P = 0.74$). However, the Kruskal–Wallis test showed a significant difference after the analysis of left breast images ($P < 0.05$), whereas the Steel–Dwass multiple-comparison test showed a significant difference only between the novel method and TOPUP ($P < 0.05$). Without PI in the right breast, significant differences were observed in the Kruskal–Wallis test ($P < 0.01$), whereas no significant differences were observed only for non-correction and novel methods ($P = 0.86$). In the left breast, significant difference in the Kruskal–Wallis test ($P < 0.01$) was observed, whereas no significant differences were observed only for non-correction and novel methods ($P = 0.61$) (Fig. 8).

4. Discussion

Breast concavities arise from shrinkage caused by aging [12] and lead to non-uniform fat suppression [6]. The fat-suppressed effect was influenced by the magnetic field's inhomogeneity due to surrounding air. Therefore, the EPI image also influenced the distortion of phase dispersion in EPI. For researchers seeking to physically assess an image with correction, a breast phantom that could easily reveal the influence of distortion could be convenient and facilitate quantification. In cases where distortion was influenced due to air by breast phantom, distortion of any clinical situation could be managed. We used an original breast phantom that could easily reveal the influence of non-uniform fat-suppression based on clinical data [6]. We considered that strong distortion was reproduced as much as possible when we showed the clinical situation; hence, we used phantoms that were highly susceptible to distortion.

We developed a novel distortion correction method for DWI using non-rigid image registration from b0 to the anatomical image and obtained displacement field applied to b1000 image. In the proposed method, edge information was obtained by the multistage threshold to determine the fast computation time and to suppress excessive deformation. Moreover, this edge information could be obtained by assembling a plural anatomical image with various degrees of contrast. Improvement of registration accuracy could be expected to follow.

Generally, in comparison with low b value image, a high b value image is disadvantageous in terms of the anatomical information; therefore, we applied a non-rigid image to b0 image. Thus, the image distortion that arises due to eddy current by MPG cannot be corrected. We considered that the eddy-current distortion could be improved because the non-rigid image registration was applied directly to the high b value image. This novel method may be applied to any type of clinical imaging technique.

The CCC between b1000 images and FS-T1WI was calculated because the high-signal area in the b1000 image was compared with the enhanced area in FS-T1WI with contrast medium in the breast MRI to arrive at a diagnosis. The CCC was the highest, and the error was the least, as suggested by the results obtained for the novel method. The distortion was well corrected using the novel method not only with PI but also without PI; therefore, the novel method was useful. Moreover, significant difference was found between the novel method and TOPUP. Therefore, we concluded that the novel method was the superior technique.

Without PI in the right breast, the number of pixels in shape error analysis was larger than the left breast. We considered this reason because the static magnetic field (B0) was inhomogeneous. B0 inhomogeneity was related to displacement field homogeneity.

In this study, non-rigid image registration was applied directly to anatomical images. Compared with TOPUP, the proposed method achieved superior correlation with anatomical images. Moreover, we considered that the novel method could be useful when high intensity of high b value image or ADC was compared with contrast enhancement effect or relaxation time of the anatomical image using ROI measurement. Furthermore, the ADC of the novel method had a high reliability because no significant difference was found between the non-correction and novel method. A comparison between ADC before and after non-rigid image registration confirmed the potential of this novel method for application in clinical practice.

This study had certain limitations. The area of signal pile-up caused by distortion could not be restored. In such situations, using a field map in combination with TOPUP may be recommended. The distortion field in the two images is reversed: the signal pile-up regions in one image correspond to regions of signal dilution in the other image and vice versa. This provides the necessary information for the originally underdetermined system to redistribute the signals to their correct locations [13]. The novel method presented here was proven to have high accuracy, without the need for extra scans, extended scan time, or excessive patient burden. This method should be easy to apply in clinical practice. It could be not only breast MRI but also the other parts of body, which were easy to be influenced by distortion, such as the paranasal sinus.

5. Conclusion

We developed a novel technique for retrospective distortion correction based on non-rigid image registration. The high degree of accuracy of this method combined with the lack of requirement for additional scans renders it a promising tool for application in clinical practice.

Disclosure of conflicts of interest

There are no conflicts of interest to declare.

References

[1] Andre JB, Zaharchuk G, Fischbein NJ, et al. Clinical assessment of standard and generalized autocalibrating partially parallel acquisition diffusion imaging: effects of reduction factor and spatial resolution. Am. J. Neuroradiol. 2012;33:1337–42.
[2] Cusack R, Brett M, Osswald K. An evaluation of the use of magnetic field maps to undistort Echo-planar images. NeuroImage 2003;18:127–42.
[3] Wan X, Gullberg GT, Parker DL, Zeng GL. Reduction of geometric and intensity distortions in echo-planar imaging using a multireference scan. Magn. Reson. Med. 1997;37(6):932–42.
[4] Studholme C, Constable RT, Duncan JS. IEEE Trans. Med. Imaging 2000;19(11):1115–27.
[5] Li Y, Xu N, Fitzpatrick JM, Morgan VL, Pickens DR, Dawant BM. Accounting for signal loss due to dephasing in the correction of distortions in gradient-echo EPI via nonrigid registration. IEEE Trans. Med. Imaging 2007;26(12):1698–707.
[6] Takatsu Y, Nishiyama K, Miyati T, Miyano H, Kajihara M, Akasaka T. A comparison

of shimming techniques for optimizing fat suppression in MR mammography. Radiol. Phys. Technol. Jul 2013;6(2):486–91.
[7] Takatsu Y, Kyotani K, Ueyama T, Miyati T, Yamamura K, Andou A. Assessment of the quality of breast MR imaging using the modified Dixon method and frequency-selective fat suppression: a phantom study. Magn. Reson. Med. Sci. Jan 30 2018. https://doi.org/10.2463/mrms.tn.2017-0144. [In press].
[8] Thirion JP. Image matching as a diffusion process: an analogy with Maxwell's demons. Med. Image Anal. 1998;2(3):243–60.
[9] Vercauteren T, Pennec X, Perchant A, Ayache N. NeuroImage 2009;45:61–72.
[10] Andersson JL, Skare S, Ashburner J. How to correct susceptibility distortions in spin-echo echo-planar images: application to diffusion tensor imaging. NeuroImage 2003;20(2):870–88.
[11] Kanda Y. Investigation of the freely available easy-to-use software'EZR' for medical statistics. Bone Marrow Transplant. 2013;48:452–8.
[12] Regnault P. Breast ptosis definition and treatment. Clin. Plast. Surg. 1976;3(2):193–203.
[13] Irfanoglu MO, Modi P, Nayak A, Hutchinson EB, Sarlls J, Pierpoli C. DR-BUDDI (Diffeomorphic Registration for Blip-Up blip-Down Diffusion Imaging) method for correcting echo planar imaging distortions. NeuroImage 2015;106:284–99.